Energy-dependent dynamical quantum phase transitions in quasicrystals

Shihao Ye,[1] Ziheng Zhou,[1] Niaz Ali Khan,[1,2,*] and Gao Xianlong[1,†]
[1]*Department of Physics, Zhejiang Normal University, Jinhua 321004, P. R. China*
[2]*Zhejiang Institute of Photoelectronics and Zhejiang Institute for Advanced Light Source, Zhejiang Normal University, Jinhua 321004, P. R. China*

(Received 13 December 2023; revised 16 March 2024; accepted 9 April 2024; published 22 April 2024)

Recently the role of the mobility edge in localization transitions has been extensively studied for one-dimensional tight-binding quasiperiodic models. In this work we study the mobility edge in a family of quasiperiodic systems evolving far from equilibrium, such as quench dynamics. We report numerical simulations of the Loschmidt echo based on a polynomial expansion-based technique with a moderate computational cost. Remarkably, we obtain an identical energy dependence on the equilibrium and dynamical quantum phase transitions of quasiperiodic models. The self-dual energy-independent localization model under quench dynamics exhibits energy-independent dynamical quantum phase transitions. On the other hand, self-dual energy-dependent localization models undergo energy-dependent dynamical quantum phase transitions. The results provide insights into energy-dependent dynamical localization transitions in quasiperiodic systems relevant to experiments.

DOI: 10.1103/PhysRevA.109.043319

I. INTRODUCTION

The concept of mobility edges refers to critical energy values that demarcate localized states from extended states in quantum systems [1–8]. Understanding quantum transport near the mobility edge is crucial in various fields, such as condensed matter physics and materials science [7–13]. It is a well-established fact that all eigenstates in 1D and 2D disordered systems are localized, in which the disorder is represented by a random amplitude of the on-site energies [14–19]. In the 3D Anderson model, however, there is a mobility edge that separates extended states from localized states [20,21]. The mobility edge depends on the characteristics of disordered systems, such as the nature and strength of the disorder [3,21]. In comparison with random disorder systems, the standard 1D Aubry-André (AA) model [22] manifests a self-duality relation for the transformation between position and momentum spaces at the critical quasiperiodic potential, leading to an energy-independent localization transition [22–24]. Most essentially, the quasiperiodic potential periodicity of the diagonal potential is incommensurate with the lattice periodicity; it lies between the completely periodic and the random potentials regime [25]. Interestingly, a quasiperiodic potential entails Bloch states for periodic and induces an energy-independent localization transition for random potentials regime. However, the self-dual generalized Aubry-André model [3,8] and non-Hermitian [26] manifest an energy-dependent localization transition that depends on the strength of the incommensurate modulation potential. In addition, an energy-dependent localization transition has been encountered in a 1D quasiperiodic mosaic lattice [5]. Furthermore, exact mobility edges that distinguish localized states from critical states have been observed in a quasiperiodic mosaic lattice [8]. Moreover, an interaction-induced mobility edge localization transition has been experimentally observed in the atomic Aubry-André model [7]. Most recently, multimobility edges have been experimentally realized in quasiperiodic mosaic lattices [27]. Importantly, the existence of mobility edges can significantly affect the electronic, optical, and transport properties of quantum systems [28].

A quantum quench process is the simplest paradigm of nonequilibrium dynamics where rapidly changing the parameters of a quantum system takes an initial stationary state into a complicated time-evolved state [29–47]. Traditionally, quench refers to an immediate response—a fast time dependence compared to all scales of the problem—of the system to a sudden change in parameters. Quantum quench processes offer a rich playground for studying the dynamical behavior of quantum systems. They provide information on fundamental quantum phenomena, such as dynamical quantum phase transitions (DQPTs) [29,30] and the emergence of new phases of matter [47], and have practical implications for quantum technology and information processing [48–50]. Remarkably, DQPTs are a fascinating concept in quantum physics that extends the understanding of phase transitions to the realm of nonequilibrium dynamics, characterized by the zero of the Loschmidt echo (LE) at certain critical times of quenched systems [31,37]. From an experimental point of view, quantum quench processes have been observed in various physical systems, including interacting transverse field Ising models [51], ultracold atomic optical lattices [52], superconducting quantum simulators [35], and 2D Bose gas of rubidium atoms [47].

The phenomenon of DQPTs has opened up a new avenue toward a better understanding of nonequilibrium transport in 1D quasiperiodic systems. Most of the up-to-date research is devoted to DQPTs in self-dual energy-independent

*niazkhan@zjnu.edu.cn
†gaoxl@zjnu.edu.cn

localization models. However, the role of mobility edges on the DQPTs in quenched quasicrystals has not been explored. In this work, we uncover the phenomenon of dynamical quantum transports in a family of noninteracting 1D quasiperiodic lattices that undergo localization transitions with or without mobility edges. Moreover, quench dynamics is induced by an abrupt change in the diagonal incommensurate potential, and the initial plane wave is quenched into a time-evolved state of the system Hamiltonian. We take advantage of the kernel polynomial method for the numerical treatments of the LE, which enables us to explore large-scale numerical simulations of quantum quenched systems. Interestingly, we obtain similar energy dependence on the phenomenon of equilibrium and nonequilibrium localization transitions in quasicrystals. More specifically, energy-dependent localization transition models under quench dynamics manifest energy-dependent DQPTs. On the other hand, we encounter energy-independent DQPTs in self-dual quasiperiodic systems with energy-independent localization. Further, we find no energy dependence of the DQPTs in the infinite limit of the onsite potential.

The quantum quench protocols are in general the nonequilibrium dynamics between the time-independent extended (localized), $|\Psi_i\rangle$, and time-evolved localized (extended), $|\Psi_f\rangle$, states, where the prequench and postquench Hamiltonians ($\mathcal{H}_i$ and $\mathcal{H}_f$) of the systems are noncommutable, $[\mathcal{H}_i, \mathcal{H}_f] \neq 0$. However, at time $\tau = 0$, the Hamiltonian operators are commuting and share a common eigenstate, resulting in $|\langle\Psi_i|\Psi_f\rangle| = 1$. Moreover, the system does not display any signatures of DQPTs for quench dynamics between states in the same regime, where the overlap between states lies in the range $0 < |\langle\Psi_i|\Psi_f\rangle| \leqslant 1$. The main focus is to study the quench dynamics of quasiperiodic systems between the extended and time-dependent localized phases. In this case, the initial ground state is energy dependent, which is quenched into a localized regime. Subsequently, depending on the nature of the quasiperiodic model, one can trace out the emergence of the DQPTs with mobility edges. On the other hand, the AA model undergoes DQPTs when an initial localized state, $|\Psi_m\rangle = \sum_{n=1}^{N} \delta_{n,m}\hat{c}_n^\dagger|0\rangle$, is quenched into an extended regime, as reported in the literature [31,45,53].

The structure of our paper is as follows. Section II discusses tight-binding models of 1D noninteracting spinless fermions in a diagonal incommensurate potential. We also briefly review the established nonequilibrium transport formalism based on the LE. Section III focuses on the implementation of polynomial expansions for LE of quenched tight-binding models with diagonal quasiperiodic incommensurate potential. Section IV explores the DQPTs of electrons in a family of quasiperiodic chains that undergo localization transitions with or without mobility edges. The last section summarizes our conclusions.

II. MODEL AND QUENCH DYNAMICS

This section is devoted to a comprehensive study of 1D electronic systems with different local potentials and discusses the transport properties of the systems in an equilibrium setting. We emphasize the localized or extended nature of the controlling parameters of quantum systems. We also briefly discuss the quench dynamics of the system as probed by the LE.

A. Theoretical models

We first consider the paradigmatic AA model [22] introduced by Aubry and André in the 1980s. This model can be described as a chain of a single particle of noninteracting spinless electrons with nearest-neighbor hopping in a 1D lattice subjected to onsite incommensurate potential. The Hamiltonian of the system has the general form [22]

$$\mathcal{H} = -t\sum_{n=1}^{N}(\hat{c}_n^\dagger\hat{c}_{n+1} + \hat{c}_{n+1}^\dagger\hat{c}_n) + \sum_{n=1}^{N}\varepsilon_n\hat{c}_n^\dagger\hat{c}_n, \tag{1}$$

where $\hat{c}_n^\dagger$ and $\hat{c}_n$ are the free fermionic rising and lowering operators at site n, respectively. The parameter ε_n denotes the energy of an electron at the nth site, N is the lattice size, and t is the hopping integral between the nearest-neighboring sites. We measure all energy scales in units of t, which hereafter is set to unity. For the AA model, the lattice site energy is the quasiperiodic potential given by [22]

$$\varepsilon_n = \lambda\cos(2\pi\alpha n + \phi), \tag{2}$$

where λ is the strength of the incommensurate diagonal energy with $\alpha = (\sqrt{5}-1)/2$, which is an irrational number, and ϕ is the phase parameter, which is set to zero without loss of any generality. This model is known to exhibit metal-insulator transitions at $\lambda = 2t$. The states of the system are extended for $\lambda < 2t$ and localized for $\lambda > 2t$ as shown in the Appendix.

The second model we consider is the generalized Aubry-André (GAA), subjected to a different on-site quasiperiodic potential. The GAA model is an extension of the AA model with a diagonal potential given by [3,4]

$$\varepsilon_n = \lambda\frac{\cos(2\pi\alpha n + \phi)}{1 - \beta\cos(2\pi\alpha n + \phi)}, \tag{3}$$

where β is the tuning parameter defined on the interval $\beta \in (-1, 1)$, and controls the distribution of site energies. The GAA potential is a smooth function of the β and has singularities at ± 1. In the limit of $\beta = 0$, one may recover the standard AA model, leading to a localization transition at the self-dual point $\lambda = 2t$ without a mobility edge. However, for $\beta \neq 0$, the GAA model exhibits a metal-insulator transition with an exact mobility edge E_c, verified by the following analytical expression [3]:

$$\beta E_c = 2t - \lambda. \tag{4}$$

Indeed, for $\beta = 0$ the GAA model is reduced to a familiar self-dual energy-independent localization AA model with a $\lambda = 2t$ critical point. For various β, the GAA model hosts localization transitions with exact mobility edges separating the localized and extended states, as given by the analytical expression (4) [3].

The third model under consideration is the quasiperiodic mosaic Aubry-André (MAA) [5,8,27], where the argument of the cosine function in the standard AA model is modified by an integer, given by [5]

$$\varepsilon_n = \begin{cases} \lambda\cos(2\pi\alpha n + \phi), & n = m\kappa, \\ 0, & \text{otherwise}, \end{cases} \tag{5}$$

where κ is an integer determining the mosaic modulation period of the diagonal potential. We set $\phi = 0$ for convenience. It is straightforward to show that the quasiperiodic mosaic lattice reduces to a pure AA model in the limit $\kappa = 1$, as reported in the literature [22]. Introducing the mosaic parameter $\kappa \neq 1$ in the quasiperiodic potential breaks the self-duality symmetry of the models, leading to the existence of mobility edges separating localized states from extended states. The quasiperiodic mosaic lattice with $\kappa = 2$ and $\kappa = 3$ at the same modulation strength contains two and four mobility edges E_c, respectively. The analytical expressions are given by [5]

$$E_c = \begin{cases} \pm\frac{1}{\lambda}, & \kappa = 2, \\ \pm\sqrt{1 \pm \frac{1}{\lambda}}, & \kappa = 3. \end{cases} \tag{6}$$

Importantly, one can obtain $2(\kappa - 1)$ mobility edges for an integer value of κ. For $\kappa = 2$, the mosaic lattice always exhibits extended states at the band center, irrespective of the potential strength. Moreover, the localization transition starts from the band edges and moves toward the center of the spectrum with increasing potential strength with mobility edges $\pm 1/\lambda$. In the infinite potential limit ($\lambda \to \infty$), the mobility edges merge to a point. Remarkably, all eigenstates of the MAA are localized for $|E| > 1/\lambda$ and extended for $|E| < 1/\lambda$. For $\kappa = 3$, the model always exhibits an extended state near the band edges and in the limit $\lambda < 2$ with four mobility edges. In the limit of $\lambda \to \infty$, all mobility edges converge to $|E| = \pm 1$, and the system displays insulating behavior with localized eigenstates.

The fourth model of our interest is the Aubry-André-Fibonacci (AAF) model [24,54,55]. The onsite potential of the AAF is governed by smooth modulation,

$$\varepsilon_n = \lambda \frac{\tanh\{\gamma[\cos(2\pi\alpha n + \phi) - \cos(\pi\alpha)]\}}{\tanh(\gamma)}, \tag{7}$$

where γ is a tunable parameter interpolating between AA modulation and Fibonacci modulation. In the limit of $\gamma \to 0$, the AAF model reduces to the AA model with a constant energy shift, $\cos(\pi\alpha)$. In this limit, the system displays a localization transition for all eigenmodes at the critical point $\lambda = 2t$. In the opposite limit ($\gamma \to \infty$), the potential approaches the Fibonacci modulation, which corresponds to a square wave switching between ± 1. In this case, all the eigenstates of the Fibonacci model are critical for any finite $\lambda/t > 0$ [56,57]. The critical line that separates extended from localized states is obtained by self-duality mapping, written as

$$\lambda = \frac{2t}{1 - \frac{\gamma^2}{6}\cos(2\pi\alpha)}. \tag{8}$$

This expression shows that the AAF model exhibits a metal-insulator transition without a mobility edge. Furthermore, the AAF model reduces to the AA model for $\gamma = 0$ and Fibonacci model in the limit of $\gamma \to \infty$. In the Fibonacci limit ($\gamma \to \infty$), all the eigenstates of the system are always critical. The AAF model in weak γ limit displays metal-insulator transition, demarcated by the analytical expression (Eq. (8)). However, the states are always critical in the large γ limit.

B. Loschmidt echo

A LE (measured in units of lattice spacing) is defined as the measure of the overlap between the initial wavefunction and the time-evolved eigenstate of the Hamiltonian. It is applied to quantify the sensitivity of the quench dynamics of quantum systems. Quantum quench dynamics describe a sudden change or perturbation in the parameters of a system. This abrupt change typically involves altering the Hamiltonian of the system, which represents its energy and dynamics. The most common scenario for a quantum quench process involves a well-defined initial state $|\Psi(y)\rangle$ (ground state) of a system Hamiltonian $\mathcal{H}(y)$ at time $\tau = 0$, where y is a quench parameter, such as the strength of onsite potential or interaction strength. Then, suddenly changing a quench parameter at certain times, $\tau > 0$, governs the time evolution of the system as it evolves under the Hamiltonian $\mathcal{H}(z)$, where z denotes the postquench parameter. The time-evolved state is [31,33,35]

$$|\Psi(y, z, \tau)\rangle = e^{-i\tau\mathcal{H}(z)}|\Psi(y)\rangle. \tag{9}$$

From the initial ground and time-evolved state, one can calculate the Loschmidt amplitude, $\mathcal{G}(y, z, \tau)$, defined as

$$\mathcal{G}(y, z, \tau) = \langle\Psi(y)|\Psi(y, z, \tau)\rangle. \tag{10}$$

A LE, $\mathcal{L}(y, z, \tau)$, is measured as the absolute square of the complex quantity $\mathcal{G}(y, z, \tau)$ and corresponds to the dynamical analog of the return probability (ground-state fidelity), defined as [31,33,35]

$$\mathcal{L}(y, z, \tau) \equiv |\mathcal{G}(y, z, \tau)|^2 = |\langle\Psi(y)|\Psi(y, z, \tau)\rangle|^2. \tag{11}$$

Typically, the LE for the AA model oscillates at the same frequency and decays to zero periodically when an initial plane wave is quenched to a strongly localized time-evolved state [31]. The occurrence of the zeros of LE signals DQPTs. It is well established that the emergence of mobility edges is a fundamental characteristic of Anderson localization. The main focus of this study is to uncover similar phenomenology for the nonequilibrium scenario in a family of quasiperiodic systems under quench dynamics.

III. KERNEL POLYNOMIAL METHOD

The kernel polynomial method (KPM) [58–67] is a numerical technique used in condensed matter physics and quantum mechanics to compute various properties of quantum systems. It is particularly useful for studying disordered or strongly correlated systems, where numerical methods are computationally expensive and limited to small system sizes [33,68]. KPM is a polynomial expansion-based method often used to compute static thermodynamic quantities, high-resolution spectral densities, nonequilibrium dynamics [53], and zero-temperature dynamical correlations [58,59]. It can efficiently handle large system sizes, making it suitable for studying realistic condensed matter systems [58,59]. It can be applied to a variety of problems, including the study of electronic structure in disordered materials [58], the analysis of QPTs [69], and the calculation of transport properties in condensed matter systems [63,64]. The typical choice for the basis functions in KPM is a set of orthogonal Chebyshev polynomials. These polynomials are well suited for the method because of their

good numerical properties [70]. As Chebyshev polynomials are defined only in the specified domain $[-1, 1]$, one needs to rescale the system Hamiltonian and all energy scales in the corresponding range. This can be done by dividing the Hamiltonian by $2Dt + \mathcal{A}$, where D is the system's dimension and $\mathcal{A}$ is a number that imposes the spectrum to be in the interval $[-1, 1]$. The first type of Chebyshev polynomials of mth degree, $T_m(z)$ are defined on the $[-1, 1]$ by

$$T_m(z) = \cos[m \arccos(z)], \quad m \in \mathbb{N}. \tag{12}$$

Moreover, the $T_m(z)$ obeys the recurrence relation,

$$T_m(z) = 2zT_{m-1}(z) - T_{m-2}(z), \quad m > 1, \tag{13}$$

starting with $T_0(z) = 1$ and $T_1(z) = z$. The Chebyshev polynomial also satisfies the following orthogonality relation:

$$\langle T_m(z)|T_n(z)\rangle = \frac{1}{\pi}\int_{-1}^{1} \frac{T_m(z)T_n(z)}{\sqrt{1-z^2}}\,dz,$$
$$= \frac{1}{2}\delta_{m,n}(\delta_{m,0}+1).$$

The KPM expansion of the Loschmidt amplitude truncated at order M has the form [53]

$$\tilde{\mathcal{G}}(y, z, \tau) = \sum_{m=0}^{M-1} \frac{2i^{-m}}{1+\delta_{m,0}} J_m(\Omega\tau)\langle T_m[\tilde{\mathcal{H}}(z)]\rangle, \tag{14}$$

where

$$\langle T_m[\tilde{\mathcal{H}}(z)]\rangle = \langle\Psi_i|T_m[\tilde{\mathcal{H}}(z)]|\Psi_i\rangle \tag{15}$$

is the expectation value of the Chebyshev polynomials in the Hamiltonian and

$$|\Psi_i\rangle = \frac{1}{\sqrt{N}}\sum_{n=1}^{N} \exp(ikn)\hat{c}_n^\dagger|0\rangle \tag{16}$$

is the initial plane wave of wave vector k defined over interval $k \in (-\pi/a\ , \pi/a]$ with a lattice spacing a and eigenenergy $E = -2t\cos(ka)$. In expression (14), $J_0(z)$ is the zero-order Bessel function of the first kind, and $\tilde{\mathcal{H}} = \mathcal{H}/\Omega$ is the rescaled Hamiltonian of the system, where Ω is a positive energy scale that normalizes the Hamiltonian and its spectrum to the standard Chebyshev polynomial interval $[-1\ , 1]$. It is important to mention that the LE is a differentiable function; hence, the accuracy and numerical convergence of the KPM approximates of the LE can be controlled only by the polynomial moments. The expectation value of Chebyshev polynomials in the Hamiltonian [see Eq. (15)] can be evaluated very efficiently by using matrix-vector multiplication. Starting from the initial plane wave $|\Psi_i\rangle$, one can iteratively calculate the expectation value of $T_m[\tilde{\mathcal{H}}(z)]$ as follows:

$$\langle T_0[\tilde{\mathcal{H}}(z)]\rangle = \langle\Psi_i|T_0[\tilde{\mathcal{H}}(z)]|\Psi_i\rangle = 1, \tag{17}$$

$$\langle T_1[\tilde{\mathcal{H}}(z)]\rangle = \langle\Psi_i|\tilde{\mathcal{H}}(z)|\Psi_i\rangle = \langle\tilde{\mathcal{H}}(z)\rangle, \tag{18}$$

and for $m > 1$, we use the following recursion relation:

$$\langle T_m[\tilde{\mathcal{H}}(z)]\rangle = 2\langle\tilde{\mathcal{H}}(z)\rangle\langle T_{m-1}[\tilde{\mathcal{H}}(z)]\rangle - \langle T_{m-2}[\tilde{\mathcal{H}}(z)]\rangle. \tag{19}$$

In general, the LE has been evaluated by the exact diagonalization method, which has an $O(N^2)$ numerical complexity for a sparse Hamiltonian matrix of single-particle systems. In comparison, the overall computational cost of the KPM procedure is $O(MN)$ for the sparse matrix Hamiltonian. Because of matrix-vector multiplication, the most time-consuming part of this procedure is the iterative evaluation of the expectation value $\langle T_m(\tilde{\mathcal{H}}(z))\rangle$, costing $O(N)$ numerical complexity. The $O(M)$ comes from the summing over the Chebyshev series in Eq. (14). Interestingly, the KPM technique can estimate very accurate numerical data for sufficiently large Chebyshev series. Hence, the numerical accuracy, convergence, and resolution of the LE simulations are strongly controlled by the number of Chebyshev series. Nevertheless, the Chebychev-expansion approach doesn't work for an initial state with $\lambda_i > 0$ since the system's initial state won't be a plane wave [Eq. (16)] and Bloch wave functions are not applicable in quasicrystals.

IV. QUENCH DYNAMICS

In this section we uncover the quench dynamics of a family of 1D lattice models with incommensurate onsite potential, leading to a qualitative understanding of the electronic transport of quantum systems in a nonequilibrium scenario. It is important to mention that in all cases the quench dynamics are induced by an abrupt change in the strength of the incommensurate potential, where an initial plane wave (the ground state of the system Hamiltonian) is quenched in a time-evolved state. Moreover, we implement the kernel polynomial technique for the calculations of the LE of quasiperiodic models. All numerical calculations are carried out for the system's size $N = 131\,072$ and $M = 1024$ Chebyshev moments with periodic boundary conditions.

Figure 1 shows phase diagram of the standard AA model under quench dynamics. The phase diagram [Figs. 1(a)–1(c)] is obtained by calculating the LE of the quenched system, where the initial state of the Hamiltonian with (a) $\lambda_i = 0$, (b) $\lambda_i = 0.1$, (c) $\lambda_i = 0.2$ is quenched into a time-evolved state with $\lambda_f = 10^4$. More precisely, we initially prepare a ground state of the system that corresponds to any particular energy eigenstate and quench it into a time-dependent state of the system with a strong quasiperiodic potential, as given by

$$|\Psi_f\rangle = |\Psi(\lambda_i, \lambda_f, \tau)\rangle = e^{-i\tau\mathcal{H}(\lambda_f)}|\Psi_i\rangle, \tag{20}$$

where the $|\Psi_f\rangle$ time-dependent quantum state corresponds to any particular energy eigenstate, relating the state at time $\tau = 0$ with the state at time τ. It contains simultaneously all information involved in the system. As illustrated from Figs. 1(a)–1(c), for $\lambda_i < 2$ (extended regime), the system displays DQPTs without mobility edges, as characterized by singularities of the LE at certain critical times. Moreover, for an initially prepared pure system, the LE decays oscillatorily with time as $|J_0(\lambda_f\tau)|^2$ and supports singular behavior at certain critical times, $\tau^* = x_m/\lambda_f$, with m set of positive roots. Although the initial and time-evolved states are energy dependent, the LE turned out to be energy-independent. It turns out that there is a strong connection between the equilibrium and the dynamical phase transition in this model, as the AA model undergoes a quantum phase transition at critical quasiperiodic potential strength without a mobility edge. More specifically, the AA model exhibits energy-independent

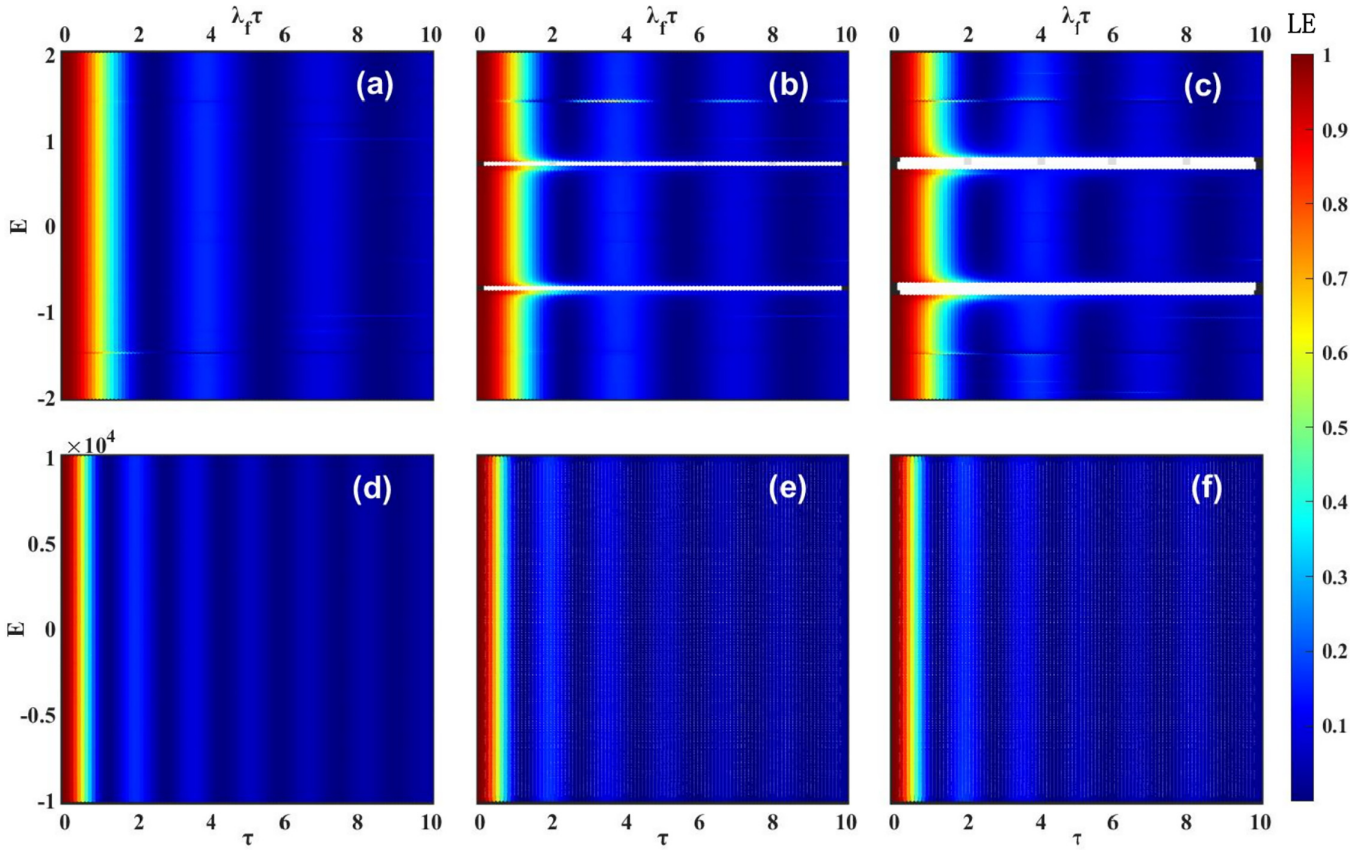

FIG. 1. Phase diagrams of the AA lattice in the energy-potential plane. Phase diagrams are obtained by calculating the LE when an initial ground state with (a) $\lambda_i = 0$, (b) $\lambda_i = 0.1$, and (c) $\lambda_i = 0.2$ is quenched into a time-evolved state with $\lambda_f = 10^4$ and when an initial localized state with $\lambda_i = 10^4$ is quenched into a time-dependent state with (c) $\lambda_f = 0$, (d) $\lambda_f = 0.1$, and (f) $\lambda_f = 0.2$. Numerical calculations are carried out for the system of size $L = 1024$ with period boundary conditions using an exact diagonalization method.

equilibrium and dynamical phase transitions. Moreover, we obtain blank spaces around $E \approx \pm 0.69$ in phase diagrams for $\lambda_i > 0$, which corresponds to the absence of the eigenspectra of the system Hamiltonian as clearly shown in the Appendix. On the other hand, Figures 1(d)–1(f) demonstrate the quench dynamics of the system when an initial localized state is quenched into an extended regime. As expected, the system displays DQPTs without mobility edges, where the LE oscillatory decays to zero in time scale.

Our main goal is to investigate the role of energy on the quench dynamics in quantum systems. Now we consider the GAA model, which exhibits energy-dependent metal-insulator transitions. After performing an abrupt change in the GAA onsite incommensurate potential, the Loschmidt amplitude [Eq. (10)] becomes

$$\mathcal{G}(E, \lambda_f, \beta, \tau) = \langle \Psi_i | e^{-i\tau \mathcal{H}(\lambda_f, \beta)} | \Psi_i \rangle. \tag{21}$$

Figures 2(a)–2(c) demonstrate the phase diagram of the GAA model for tuning parameters $\beta = 0.5$, where an initial state of the system Hamiltonian in the extended regime is quenched into a time-evolved state with $\lambda_f = 2$. It can be straightforwardly proved that the GAA reduces to the AA model at $\beta = 0$, leading to energy-independent DQPTs as shown in Fig. 1. However, for finite β, the GAA under quench dynamics for both cases undergoes an energy-dependent nonequilibrium phase transition, indicated by the zeros of the LE. It is shown that the LE tends to zero at critical times for energy $E \geqslant -1$, signaling the emergence of the DQPTs at this limit. In contrast, the system displays no DQPTs for energy $E < -1$, where the LE remains finite. It is because the time-evolved states of the system are in the extended regime for $E < -1$ but the localized regime for $E \geqslant -1$ at $\lambda_f = 2$, as clearly demonstrated in Fig. 8 below. In other words, the initial and time-dependent states are orthogonal (nonorthogonal) for $E \geqslant -1$ ($E < -1$) at critical times, reflecting the emergence (disappearance) of the DQPTs. Moreover, for $\lambda_i > 0$, we obtain blank spaces around $E \approx \pm 0.69$ in phase diagrams, which corresponds to the absence of the eigenspectra of the system Hamiltonian as clearly shown in the Appendix. On the other hand, Figs. 2(d)–2(f) demonstrate the quench dynamics of the system when an initial state with $\lambda_i = 2$ is quenched into time-dependent extended state. As expected, the system displays DQPTs for energy $E \geqslant -1$, where the LE decays to zero in timescale. However, the LE remains finite for $E \leqslant -1$, signaling the disappearance of the DQPTs. Furthermore, we observed gaps in the phase diagram of the quench dynamics, reflecting the absence of eigenenergy of the model, as shown in the Appendix.

The origin of the occurrence of the DQPTs is the overlap between the initial plane wave and the time-evolved state of the system Hamiltonian in the localized regime. The overlap between the initial plane wave and its time-evolved state

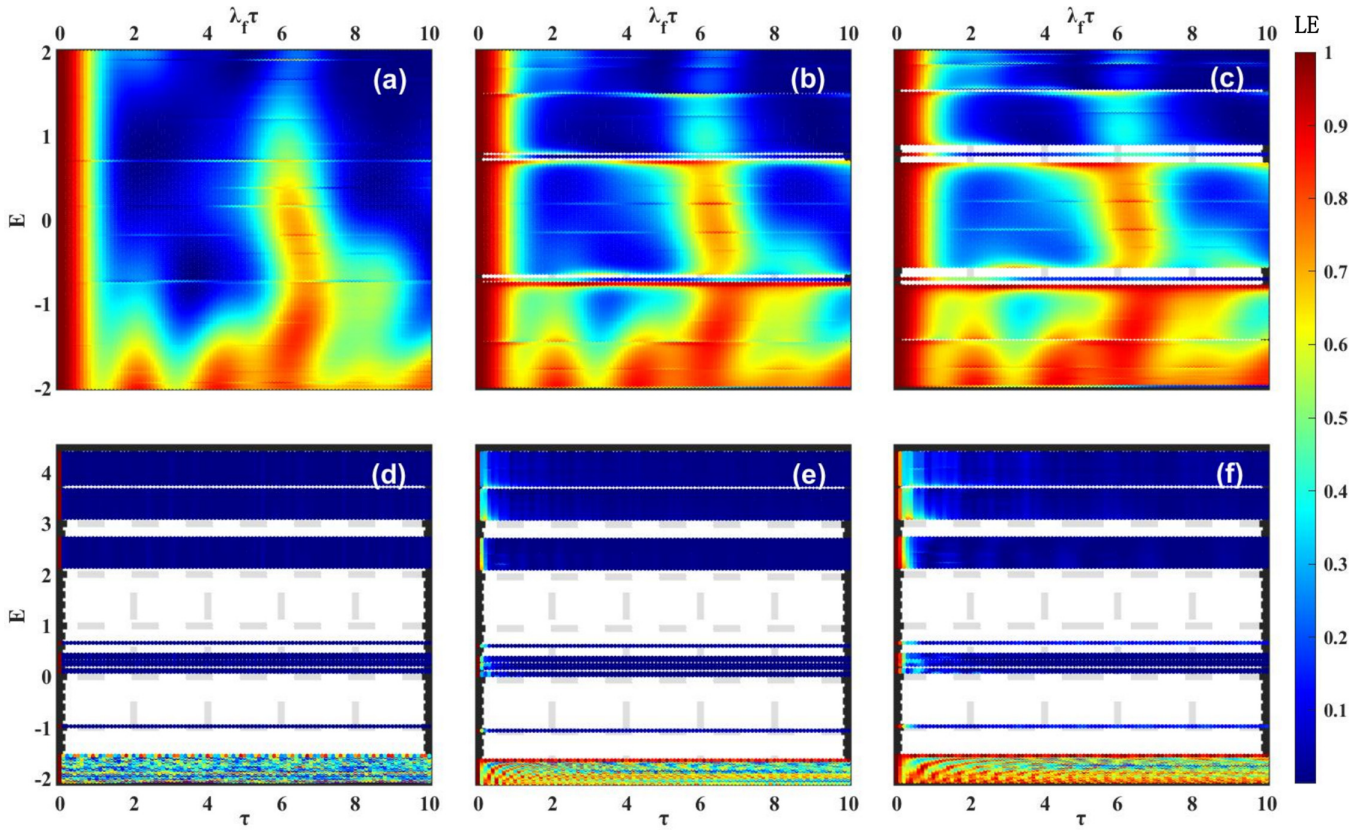

FIG. 2. Phase diagrams of the GAA lattice with $\beta = 0.5$ in the energy-potential plane. Phase diagrams are obtained by calculating the LE when an initial ground state with (a) $\lambda_i = 0$, (b) $\lambda_i = 0.1$, and (c) $\lambda_i = 0.2$ is quenched into a time-evolved state with $\lambda_f = 2$ and when an initial eigenstate with $\lambda_i = 2$ is quenched into a time-dependent state with (c) $\lambda_f = 0$, (d) $\lambda_f = 0.1$, and (f) $\lambda_f = 0.2$. Numerical calculations are carried out for the system of size $L = 512$ with period boundary conditions using an exact diagonalization method.

of the system Hamiltonian in the extended regime results in a finite LE at a certain time interval. Moreover, the LE turns out to be asymmetric with respect to $E = 0$ for $\beta \neq 0$, i.e., $\mathcal{L}(E, \lambda_f, \beta, \tau) \neq \mathcal{L}(-E, \lambda_f, \beta, \tau)$. Furthermore, when the initial state is quenched into a strongly disordered regime, then all the eigenstates $|\Psi_m\rangle$ of the quenched system are localized with spectrum E_m, given by

$$E_m = \lambda_f \frac{\cos(2\pi\alpha m)}{1 - \beta\cos(2\pi\alpha m)}. \tag{22}$$

In this case, the $\mathcal{G}(E, \lambda_f, \beta, \tau)$ [see Eq. (21)] turns out to be

$$\begin{aligned}\mathcal{G}(E, \lambda_f, \beta, \tau) &= \frac{1}{N}\sum_{m=1}^{N}\langle\Psi_i|e^{-i\tau\mathcal{H}(\lambda_f,\beta)}|\Psi_m\rangle\langle\Psi_m|\Psi_i\rangle,\\ &= \frac{1}{N}\sum_{m=1}^{N}\langle\Psi_i|\Psi_m\rangle\langle\Psi_m|\Psi_i\rangle e^{-i\tau E_m},\\ &= \frac{1}{N}\sum_{m=1}^{N}|\langle\Psi_m|\Psi_i\rangle|^2 e^{-i\tau\lambda_f\frac{\cos(2\pi\alpha m)}{1-\beta\cos(2\pi\alpha m)}},\\ &= \frac{1}{N}\sum_{m=1}^{N}|\langle\Psi_m|\Psi_i\rangle|^2 e^{-i\tau\lambda_f\frac{\cos(\theta)}{1-\beta\cos(\theta)}},\end{aligned} \tag{23}$$

where $\theta = 2\pi\alpha m$ is the phase, which is randomly distributed between $-\pi$ and π for an irrational number α in the thermodynamic limit. Moreover, the overlap amplitude of the plane wave $|\Psi_i\rangle$ and the localized state $|\Psi_m\rangle$ (localized at a single site m) becomes

$$|\langle\Psi_m|\Psi_i\rangle|^2 \approx 1. \tag{24}$$

In this limit, the Loschmidt amplitude (23) becomes

$$\mathcal{G}(E, \lambda_f \to \infty, \beta, \tau) = \frac{1}{2\pi}\int_{-\pi}^{\pi} d\theta e^{-i\tau\lambda_f\frac{\cos(\theta)}{1-\beta\cos(\theta)}}. \tag{25}$$

This expression [Eq. (25)] can be solved numerically for the calculations of the Loschmidt amplitude. The corresponding LEs for various β are shown in Fig. 3. The LE can be straightforwardly reduced to $|J_0(\lambda_f\tau)|^2$ at the limit of $\beta = 0$, indicating DQPTs at critical times. One can clearly see that the parameter β increases the frequency of the oscillations and destroys the DQPTs within a short time limit. However, the LE decays to zero periodically in the infinite time limit, as depicted in Fig. 3 (inset). The tail of the LE is very well fitted to a line (magenta dashed line) in log-log scale. This shows that the LE approaches zero in the infinitely evolving time limit. More importantly, the DQPTs turned out to be energy-dependent analogously to equilibrium phase transitions in the model.

Turning to the case when an initial plane wave is quenched into a time-evolved state of the system Hamiltonian with onsite mosaic quasiperiodic potential, Fig. 4 demonstrates the nonequilibrium dynamics of the mosaic quasiperiodic lattice

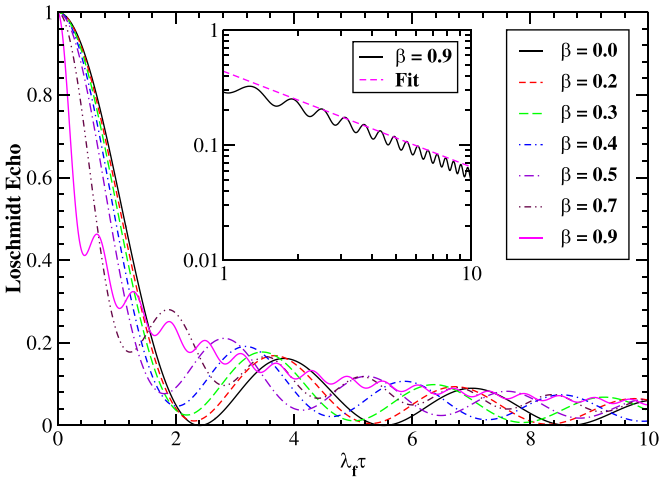

FIG. 3. LE of the GAA lattice when a plane wave is quenched into the time-evolved state with strong potential modulation $\lambda_f \to \infty$ in the thermodynamic limit. Inset: LE as a function of rescaled evolving time for $\beta = 0.9$ in log-log scale. The oscillatory decay of LE is very well fitted with a line, $y = ax$, where a is a fitting parameter.

with system size $N = 131\,072$ for $\kappa = 2$ (upper panel) and $\kappa = 3$ (lower panel) at postquench potential $\lambda_f = 3$. We observe that the LE is symmetric with respect to $E = 0$ for various κ, that is,

$$\mathcal{L}(E, \lambda_f, \kappa, \tau) = \mathcal{L}(-E, \lambda_f, \kappa, \tau). \tag{26}$$

For $\kappa = 2$, the system displays DQPTs in different manners as compared to the AA model, where the LE decays to zero periodically with different amplitudes. Moreover, the MAA undergoes an energy-dependent DQPT, as shown in Fig. 4(a). The LE decays to zero around band edges $E = \pm 2$, where all the energy eigenstates of the postquench Hamiltonian are localized as presented in [5]. However, LE remains finite at the band center $E = 0$, where the postquench system is extended in nature. On the other hand, the DQPTs turned out to be energy dependent for $\kappa = 3$, where the dynamical localization transitions happen at the band center and band edges. It is the consequences of the localized nature of the postquench system at $E = 0$ and $E = \pm 2$, as reported in [5]. At $E = \pm 1$, the system is extended in nature, and hence, its overlap with the plane wave turned out to be a nonvanishing finite value. Interestingly, the LE decays oscillatory to zeros at $E = 0$ both for $\kappa = 2$ and 3, reflecting the phenomenon of nonequilibrium phase transitions in the system. In the strong potential limit ($\lambda_f \to \infty$), the LE turns out to be $\kappa-$ and energy independent, as given by

$$\mathcal{L}(E, \lambda_f, \kappa, \tau) = |J_0(\lambda_f \tau)|^2 \tag{27}$$

in the thermodynamic limit. Here $J_0(x_s)$ is the zero-order Bessel function of the first kind and has a series of zeros x_s with $s \in \mathbb{N}$ set of positive roots. In this limit, the time-evolved state of the system Hamiltonian is in the strongly localized regime. Hence, the overlap between the initial plane wave and strongly localized time-evolved state approaches zero periodically at the timescale, resulting in DQPTs in the system. In addition, the system undergoes identical energy-dependent

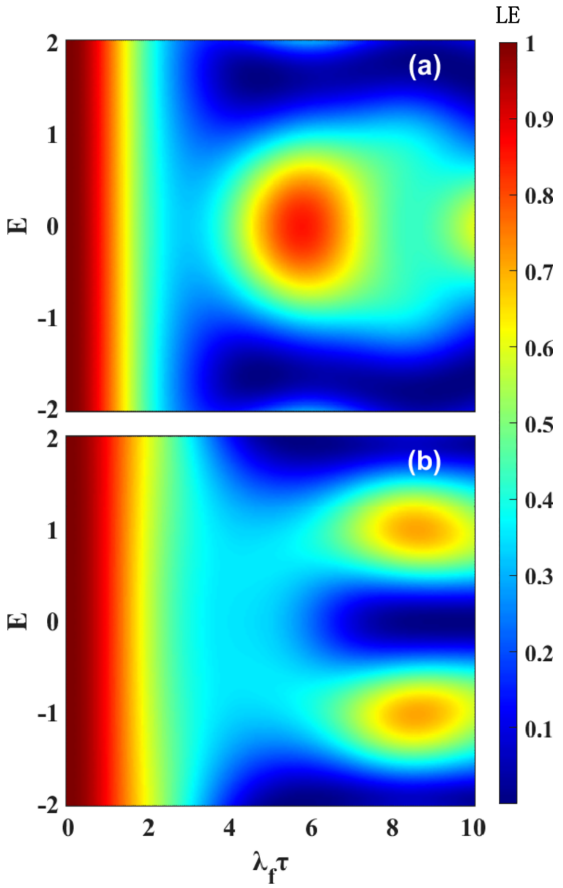

FIG. 4. Phase diagram of the MAA model in the $E - \lambda_f\tau$ plane for (a) $\kappa = 2$, and (b) $\kappa = 3$ with $\lambda_f = 3$. The phase diagram is obtained by computing the KPM estimates of the LE of the system of size $N = 131\,072$ with $M = 1024$ Chebyshev moments.

equilibrium and the nonequilibrium phase transition in this model.

We now focus on the quench dynamics of the AAF lattice system, where the tunable parameter γ interpolates between the AA and Fibonacci lattice systems. Similar to previous cases, the initial plane wave is quenched into a time-evolved state of the system Hamiltonian with different γ and postquench potentials. Again, the quench dynamics is characterized by an abrupt change in the incommensurate potential. In the limit of AA model ($\gamma = 0$), the LE oscillatory decays to zero with evolving time for strong potential modulation ($\lambda_f \to \infty$), reflecting the phenomenon of nonequilibrium phase transitions, as shown in Fig. 1(a). The quench dynamics under the AAF model for various γ and λ_f is illustrated in Fig. 5. In the approximately AA model limit ($\gamma = 1$) with $\lambda_f = 2$, the LE of the AAF goes to zero within the energy range ($-2 < E < 1$), whereas it remains finite at the band edges $E > 1$, as shown in Fig. 5(a). However, for the strong $\gamma \gg 1$ limit, the LE approaches zero within the energy range ($-2 < E < 2$), whereas it remains finite at the band edges $E \pm 2$, as shown in Figs. 5(b) and 5(c). As a consequence, the system exhibits DQPTs in the energy range ($-2 < E < 2$), as indicated by the vanishing values of the LE. On the other hand, in the strong potential limit ($\lambda_f \to \infty$), the LE is independent of energy and always decays to zero periodically,

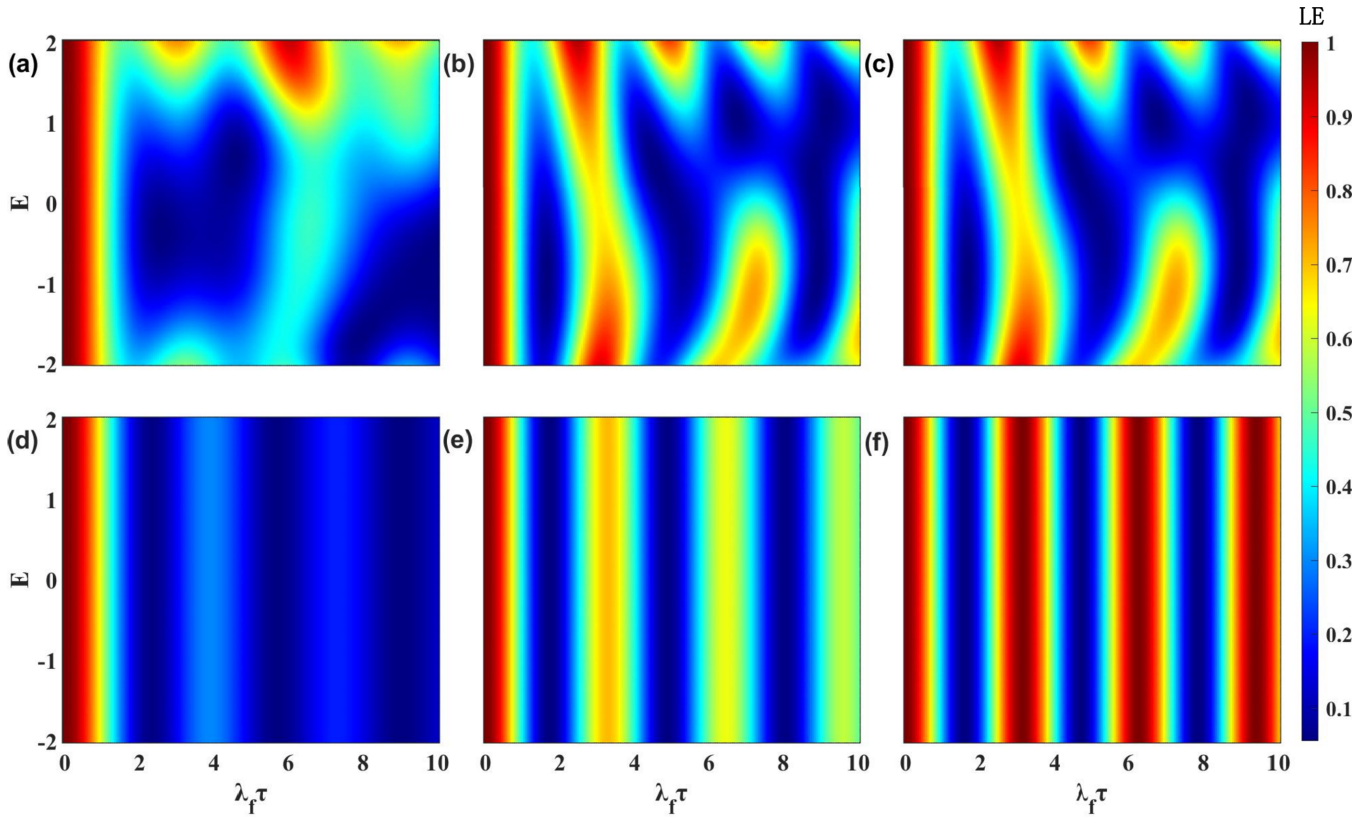

FIG. 5. Phase diagrams of the AAF lattice in the E-$\lambda_f\tau$ plane. Phase diagrams are obtained by computing the KPM estimates of the LE when an initial ground state ($\lambda_i = 0$) is quenched into a time-evolved state for (a) $\gamma = 1$, (b) $\gamma = 5$, and (c) $\gamma \to \infty$ with $\lambda_f = 2$ and (d) $\gamma = 1$, (e) $\gamma = 5$, and (f) $\gamma \to \infty$ with $\lambda_f = \infty$.

as shown in Figs. 5(d)–5(f). It is noted that the amplitude of the LE increases with increasing γ. In the limit of the Fibonacci modulation ($\gamma \to \infty$), the LE shows an interesting periodic oscillatory behavior with amplitude varying between one and zero, as explicitly depicted in Fig. 6. In the limit of the AA model ($\gamma \to 0$), the LE turns out to be $|J_0(\lambda_f\tau)|^2$. It is worth mentioning that the tuning parameter γ speeds up the appearance of the DQPTs, where the LE approaches zero faster compared to the quench dynamics in the AA model. Remarkably, the LE varies as $\cos^2(\lambda_f\tau)$ in the Fibonacci limit, $\gamma \to \infty$. In this limit, the LE oscillates between one and zero with a constant frequency on the timescale. Moreover, the zeros of LE occur at critical time, $\tau^* = (2m+1)\frac{\pi}{4}$, with $m \in \mathbb{Z}$, reflecting the existence of the DQPTs.

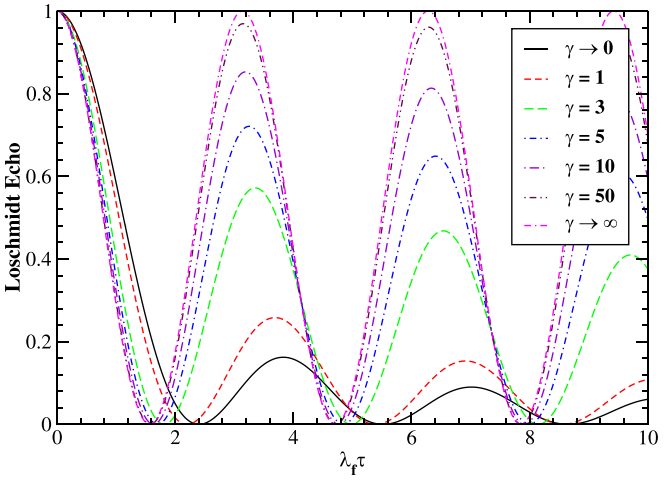

FIG. 6. LE of the AAF model when a plane wave quenched into the time-evolved state of the Hamiltonian with a strongly potential modulation $\lambda_f \to \infty$ in the thermodynamic limit.

Our main concern is to explore the role of energy on the DQPTs in 1D, noninteracting Hermitian quasicrystals. However, a fascinating road map of research is to study quench dynamics under non-Hermitian quasiperiodic lattices and induce topological phase transitions due to the interplay between non-Hermiticity and disorder. The quantum quench dynamics provides new scientific insights into the dynamical quantum transport in the topological regime of quantum systems.

V. CONCLUSION

We explored the phenomenon of nonequilibrium phase transition in a family of quasiperiodic chains restricted to nearest-neighbor interactions. A linear-scale simulation method—the kernel polynomial method—is employed for the numerical calculations of the LE, which has $O(N)$ numerical complexity. We pointed out a strong connection between equilibrium and the nonequilibrium DQPTs regarding energy dependence. Importantly, systems that undergo an energy-dependent localization transition turned

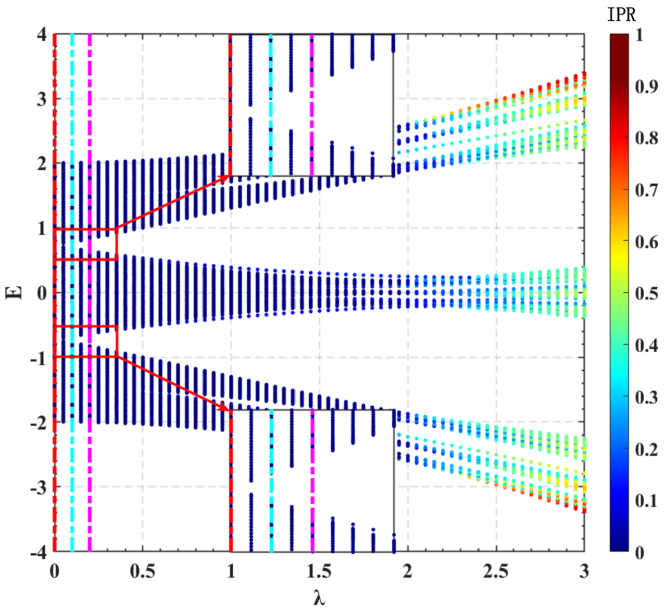

FIG. 7. Phase diagram of the AA model in the E-λ plane. The diagram is obtained by computing the IPR of the system of size $L = 1024$. The red, blue, and magenta dashed lines at $\lambda = 0$, $\lambda = 0.1$, and $\lambda = 0.2$ correspond to the data presented in Fig. 1 for the quench dynamics. In insets we enlarge the region around $E \approx \pm 0.69$ to show that the system displays no eigenenergy for $\lambda > 0$.

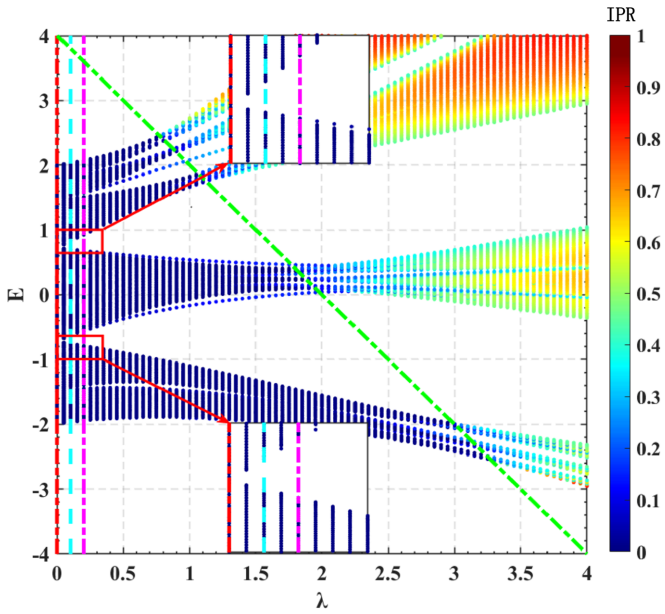

FIG. 8. Phase diagram of the GAA model in the E-λ plane. The diagram is obtained by computing the IPR of the system of size $L = 1024$. The red, blue, and magenta dashed lines at $\lambda = 0$, $\lambda = 0.1$, and $\lambda = 0.2$ correspond to the data presented in Fig. 2 for the quench dynamics. The green dashed line represents the mobility edge separating extended and localized regimes. In insets we show that the system displays no eigenenergy for $\lambda > 0$ around $E \approx \pm 0.69$.

out to exhibit an energy-dependent dynamical phase transition under the quenching process. Analogously, energy-independent localization lattice models undergo energy-independent nonequilibrium transitions. For instance, self-dual energy-independent localization models are found to display energy-independent DQPTs, whereas quasicrystals with mobility edges undergo energy-dependent DQPTs under the quenching process. However, in the strong quasiperiodic potential limit, all systems displayed energy-independent equilibrium or nonequilibrium localization transitions. Moreover, Loschmidt echo is found to have symmetric behavior with respect to energy, for both the standard and mosaic AA models, and asymmetric for the generalized AA model. However, the Aubry-André-Fibonacci model has a rather complex dependence on energy and turned out to be symmetric in the AA or Fibonacci modulation limit with infinite onsite potential and asymmetric in the finite potential limit. Our work uncovers a variety of quasiperiodic models with mobility edges and opens up an avenue for exploring the dynamical quantum transport of quantum systems with experimental feasibility.

ACKNOWLEDGMENTS

N.A.K. acknowledges the postdoctoral fellowship supported by Zhejiang Normal University under Grant No. ZC304022980. G.X. acknowledges support from the NSFC under Grant No. 12174346.

APPENDIX

To explicitly verify the phenomenon of the localization transition, we numerically calculate the inverse participation ratio (IPR),

$$\mathrm{IPR}_i = \frac{\sum_j |\psi_i(j)|^4}{\left(\sum_j |\psi_i(j)|^2\right)^2}, \tag{A1}$$

which is the most reliable theoretical tool to characterize the Anderson transition. In general, the IPR is a dimensionless quantity, proportional to $1/N$ for an extended state, whereas it tends toward unity in a strongly localized state of the system. Importantly, the AA model exhibits an energy-independent localization transition at critical potential strength $\lambda = 2t$, as depicted in Fig. 7. The vertical dashed lines at $\lambda = 0$, 0.1, and 0.2 correspond to the data presented in Figs. 1(a)–1(c). Most importantly, for $\lambda > 0$, the system yields no eigenenergy as clearly shown by zooming in the data around $E \approx \pm 0.69$. As a consequence, we obtain a blank space in the phase diagram of the quench dynamics.

Figure 8 demonstrates the phase diagram of the GAA model in the energy-potential plane. The data are computed for a system of size 1024 with periodic boundary conditions. It is pointed out that the model undergoes a metal-insulator transition with a mobility edge of $\beta E_c = 2t - \lambda$ [3]. Furthermore, the insets demonstrate that the system yields no eigenenergy around $E \approx \pm 0.69$, leaving gaps in the phase diagram of the quench dynamics.

[1] N. Mott, J. Phys. C: Solid State Phys. **20**, 3075 (1987).
[2] S. Das Sarma, S. He, and X. C. Xie, Phys. Rev. Lett. **61**, 2144 (1988).
[3] S. Ganeshan, J. H. Pixley, and S. Das Sarma, Phys. Rev. Lett. **114**, 146601 (2015).
[4] F. A. An, K. Padavić, E. J. Meier, S. Hegde, S. Ganeshan, J. H. Pixley, S. Vishveshwara, and B. Gadway, Phys. Rev. Lett. **126**, 040603 (2021).
[5] Y. Wang, X. Xia, L. Zhang, H. Yao, S. Chen, J. You, Q. Zhou, and X.-J. Liu, Phys. Rev. Lett. **125**, 196604 (2020).
[6] Y. Wang, X. Xia, Y. Wang, Z. Zheng, and X.-J. Liu, Phys. Rev. B **103**, 174205 (2021).
[7] Y. Wang, J.-H. Zhang, Y. Li, J. Wu, W. Liu, F. Mei, Y. Hu, L. Xiao, J. Ma, C. Chin, and S. Jia, Phys. Rev. Lett. **129**, 103401 (2022).
[8] X.-C. Zhou, Y. Wang, T.-F. J. Poon, Q. Zhou, and X.-J. Liu, Phys. Rev. Lett. **131**, 176401 (2023).
[9] T. Xiao, D. Xie, Z. Dong, T. Chen, W. Yi, and B. Yan, Sci. Bull. **66**, 2175 (2021).
[10] A. H. Karamlou, J. Braumüller, Y. Yanay, A. Di Paolo, P. M. Harrington, B. Kannan, D. Kim, M. Kjaergaard, A. Melville, S. Muschinske *et al.*, npj Quantum Inf. **8**, 35 (2022).
[11] Y. Xing, L. Qi, X. Zhao, Z. Lü, S. Liu, S. Zhang, and H.-F. Wang, Phys. Rev. A **105**, 032443 (2022).
[12] R. Yousefjani and A. Bayat, Phys. Rev. B **107**, 045108 (2023).
[13] S. Longhi, Phys. Rev. B **108**, 064206 (2023).
[14] P. W. Anderson, Phys. Rev. **109**, 1492 (1958).
[15] R. Balian, R. Maynard, and G. Toulouse, *Ill-Condensed Matter* (North-Holland, Amsterdam, 1984).
[16] P. A. Lee and T. V. Ramakrishnan, Rev. Mod. Phys. **57**, 287 (1985).
[17] F. Evers and A. D. Mirlin, Rev. Mod. Phys. **80**, 1355 (2008).
[18] J. P. Santos Pires, N. A. Khan, J. M. Viana Parente Lopes, and J. M. B. Lopes dos Santos, Phys. Rev. B **99**, 205148 (2019).
[19] N. A. Khan and S. T. Amin, Phys. Scr. **96**, 045812 (2021).
[20] E. Abrahams, P. W. Anderson, D. C. Licciardello, and T. V. Ramakrishnan, Phys. Rev. Lett. **42**, 673 (1979).
[21] G. Semeghini, M. Landini, P. Castilho, S. Roy, G. Spagnolli, A. Trenkwalder, M. Fattori, M. Inguscio, and G. Modugno, Nat. Phys. **11**, 554 (2015).
[22] S. Aubry and G. André, Ann. Israel Phys. Soc. **133**, 3 (1980).
[23] S. Y. Jitomirskaya, Ann. Math. **150**, 1159 (1999).
[24] V. Goblot, A. Štrkalj, N. Pernet, J. L. Lado, C. Dorow, A. Lemaître, L. Le Gratiet, A. Harouri, I. Sagnes, S. Ravets *et al.*, Nat. Phys. **16**, 832 (2020).
[25] D. R. Grempel, S. Fishman, and R. E. Prange, Phys. Rev. Lett. **49**, 833 (1982).
[26] D. Peng, S. Cheng, and G. Xianlong, Phys. Rev. B **107**, 174205 (2023).
[27] J. Gao, I. M. Khaymovich, X.-W. Wang, Z.-S. Xu, A. Iovan, G. Krishna, A. V. Balatsky, V. Zwiller, and A. W. Elshaari, arXiv:2306.10829 [cond-mat.dis-nn].
[28] C. Chiaracane, M. T. Mitchison, A. Purkayastha, G. Haack, and J. Goold, Phys. Rev. Res. **2**, 013093 (2020).
[29] M. Heyl, Phys. Rev. Lett. **115**, 140602 (2015).
[30] M. Heyl, Rep. Prog. Phys. **81**, 054001 (2018).
[31] C. Yang, Y. Wang, P. Wang, X. Gao, and S. Chen, Phys. Rev. B **95**, 184201 (2017).
[32] L. Zhou, Q.-H. Wang, H. Wang, and J. Gong, Phys. Rev. A **98**, 022129 (2018).
[33] H. Yin, S. Chen, X. Gao, and P. Wang, Phys. Rev. A **97**, 033624 (2018).
[34] A. Mitra, Annu. Rev. Condens. Matter Phys. **9**, 245 (2018).
[35] K. Xu, Z.-H. Sun, W. Liu, Y.-R. Zhang, H. Li, H. Dong, W. Ren, P. Zhang, F. Nori, D. Zheng *et al.*, Sci. Adv. **6**, eaba4935 (2020).
[36] X. Tong, Y.-M. Meng, X. Jiang, C. Lee, Gentil Dias de Moraes Neto, and G. Xianlong, Phys. Rev. B **103**, 104202 (2021).
[37] Z. Xu and S. Chen, Phys. Rev. A **103**, 043325 (2021).
[38] R. Hamazaki, Nat. Commun. **12**, 5108 (2021).
[39] T. Nag, V. Juričić, and B. Roy, Phys. Rev. Res. **1**, 032045(R) (2019).
[40] J. Naji, R. Jafari, L. Zhou, and A. Langari, Phys. Rev. B **106**, 094314 (2022).
[41] R. Jafari, A. Akbari, U. Mishra, and H. Johannesson, Phys. Rev. B **105**, 094311 (2022).
[42] Z. Liu, A. C. Balram, Z. Papić, and A. Gromov, Phys. Rev. Lett. **126**, 076604 (2021).
[43] M. Van Damme, T. V. Zache, D. Banerjee, P. Hauke, and J. C. Halimeh, Phys. Rev. B **106**, 245110 (2022).
[44] S. De Nicola, A. A. Michailidis, and M. Serbyn, Phys. Rev. B **105**, 165149 (2022).
[45] N. A. Khan, P. Wang, M. Jan, and G. Xianlong, Sci. Rep. **13**, 9470 (2023).
[46] N. A. Khan, X. Wei, S. Cheng, M. Jan, and G. Xianlong, Phys. Lett. A **475**, 128880 (2023).
[47] S. Sunami, V. P. Singh, D. Garrick, A. Beregi, A. J. Barker, K. Luksch, E. Bentine, L. Mathey, and C. J. Foot, Science **382**, 443 (2023).
[48] A. J. Daley, H. Pichler, J. Schachenmayer, and P. Zoller, Phys. Rev. Lett. **109**, 020505 (2012).
[49] X. Chen, Y. Li, Z. Wu, R. Liu, Z. Li, and H. Zhou, Phys. Rev. A **103**, 042429 (2021).
[50] Y.-X. Wang and A. A. Clerk, Nat. Commun. **12**, 6528 (2021).
[51] P. Jurcevic, H. Shen, P. Hauke, C. Maier, T. Brydges, C. Hempel, B. P. Lanyon, M. Heyl, R. Blatt, and C. F. Roos, Phys. Rev. Lett. **119**, 080501 (2017).
[52] N. Flaschner, D. Vogel, M. Tarnowski, B. S. Rem, D.-S. Luhmann, M. Heyl, J. C. Budich, L. Mathey, K. Sengstock, and C. Weitenberg, Nat. Phys. **14**, 265 (2018).
[53] N. A. Khan, W. Chen, M. Jan, and G. Xianlong, Comput. Phys. Commun. **299**, 109132 (2024).
[54] Y. E. Kraus and O. Zilberberg, Phys. Rev. Lett. **109**, 116404 (2012).
[55] M. Verbin, O. Zilberberg, Y. E. Kraus, Y. Lahini, and Y. Silberberg, Phys. Rev. Lett. **110**, 076403 (2013).
[56] M. Kohmoto, L. P. Kadanoff, and C. Tang, Phys. Rev. Lett. **50**, 1870 (1983).
[57] S. Ostlund, R. Pandit, D. Rand, H. J. Schellnhuber, and E. D. Siggia, Phys. Rev. Lett. **50**, 1873 (1983).
[58] A. Weiße, G. Wellein, A. Alvermann, and H. Fehske, Rev. Mod. Phys. **78**, 275 (2006).
[59] S. M. João, M. Andelkovic, L. Covaci, T. G. Rappoport, J. M. V. P. Lopes, and A. Ferreira, R. Soc. Open Sci. **7**, 191809 (2020).
[60] Z. Fan, J. H. Garcia, A. W. Cummings, J. E. Barrios-Vargas, M. Panhans, A. Harju, F. Ortmann, and S. Roche, Phys. Rep. **903**, 1 (2021).

[61] S. M. João, J. M. V. P. Lopes, and A. Ferreira, J. Phys. Materials **5**, 045002 (2022).
[62] A. Bjelcic, T. Niksic, and Z. Drmac, Comput. Phys. Commun. **280**, 108477 (2022).
[63] J. E. Sobczyk and A. Roggero, Phys. Rev. E **105**, 055310 (2022).
[64] S. G. de Castro, A. Ferreira, and D. A. Bahamon, Phys. Rev. B **107**, 045418 (2023).
[65] Y. Li, Z. Zhan, X. Kuang, Y. Li, and S. Yuan, Comput. Phys. Commun. **285**, 108632 (2023).
[66] P.-Y. Zhao, K. Ding, and S. Yang, Phys. Rev. Res. **5**, 023026 (2023).
[67] N. A. Khan, Chin. J. Phys. **85**, 733 (2023).
[68] M. Fadel, A. Usui, M. Huber, N. Friis, and G. Vitagliano, Phys. Rev. Lett. **127**, 010401 (2021).
[69] J. H. Pixley, P. Goswami, and S. Das Sarma, Phys. Rev. B **93**, 085103 (2016).
[70] J. Mason and D. Handscomb, *Chebyshev Polynomials* (CRC Press, New York, 2002).